



**HAL**  
open science

## Amino-grafting of montmorillonite improved by acid activation and application to the electroanalysis of catechol

Liliane Dongmo, Sherman L.Z. Jiokeng, Chancellin Pecheu, Alain Walcarius, Ignas Tonle

► **To cite this version:**

Liliane Dongmo, Sherman L.Z. Jiokeng, Chancellin Pecheu, Alain Walcarius, Ignas Tonle. Amino-grafting of montmorillonite improved by acid activation and application to the electroanalysis of catechol. *Applied Clay Science*, 2020, 191, pp.105602. 10.1016/j.clay.2020.105602 . hal-02981476

**HAL Id: hal-02981476**

**<https://hal.univ-lorraine.fr/hal-02981476>**

Submitted on 26 Nov 2020

**HAL** is a multi-disciplinary open access archive for the deposit and dissemination of scientific research documents, whether they are published or not. The documents may come from teaching and research institutions in France or abroad, or from public or private research centers.

L'archive ouverte pluridisciplinaire **HAL**, est destinée au dépôt et à la diffusion de documents scientifiques de niveau recherche, publiés ou non, émanant des établissements d'enseignement et de recherche français ou étrangers, des laboratoires publics ou privés.

# 1 Amino-grafting of montmorillonite improved by acid activation and application 2 to the electroanalysis of catechol

3 Liliane M. Dongmo<sup>a</sup>, Sherman L. Z. Jiokeng<sup>a,b</sup>, Chancellin N. Pecheu<sup>a</sup>, Alain Walcarius<sup>b</sup> and Ignas K.  
4 Tonle<sup>a,\*</sup>

5 <sup>a</sup>*Electrochemistry and Chemistry of Materials, Department of Chemistry, University of Dschang, P.O. Box 67*  
6 *Dschang, Cameroon*

7 <sup>b</sup>*Laboratoire de Chimie Physique et Microbiologie pour les Matériaux et l'Environnement (LCPME), UMR*  
8 *7564 CNRS – Université de Lorraine; 405, rue de Vandœuvre, 54600 Villers-lès-Nancy, France*

9  
10

## 11 Abstract

12 In this work, a natural sodium-montmorillonite clay mineral (Mt-Na) was functionalized  
13 with amine groups, either by direct grafting (Mt-NH<sub>2</sub>) or via acid activation followed by  
14 grafting (MtH-NH<sub>2</sub>) of [3(2-aminoethyl)amino]propyltrimethoxysilane (AEP-TMS). The  
15 morphology and structure of the resulting composite materials were characterized by scanning  
16 electron microscopy, X-ray diffraction, N<sub>2</sub> adsorption-desorption isotherms (BET method)  
17 infrared spectroscopy, CHN elemental analysis and thermogravimetric analyses (TGA). The  
18 obtained organoclays were then used to modify the surface of a glassy carbon electrode  
19 (GCE), and the permselectivity and accumulation properties of the resulting films were  
20 investigated by cyclic voltammetry (CV) and electrochemical impedance spectroscopy (EIS).  
21 The results indicated that MtH-NH<sub>2</sub> modified GCE (GCE/MtH-NH<sub>2</sub>) exhibited some charge  
22 selectivity features and can be applied to the electrochemical oxidation of catechol (CT). By  
23 plotting the double logarithmic variation of anodic peak currents (*I*<sub>pa</sub>) *versus* potential scan  
24 rate, the obtained slope value of 0.49 revealed a diffusion-controlled electron-transfer  
25 mechanisms for the redox process. The electrochemical behavior of CT on the modified  
26 electrode was also studied using differential pulse voltammetry (DPV). The sensitivities of  
27 GCE/MtH-NH<sub>2</sub> for CT were 1.71, 3.87 and 1.35-fold greater than signals obtained on the bare  
28 GCE, GCE/Mt-Na and GCE/Mt-NH<sub>2</sub> respectively, due to the ability of the aminated materials  
29 to strongly accumulate CT. After optimization, GCE/MtH-NH<sub>2</sub> was used for CT  
30 determination by differential pulse voltammetry that gave rise to a linear response in the  
31 concentration range from 5 μM to 80 μM ( $R^2 = 0.999$ ), and to a detection limit of 0.65 μM.  
32 The proposed method was applied to CT detection in water samples and in a tea sample.

33 **Keywords:** Montmorillonite, Acid activation, Grafting, Organoclays, Electroanalysis,  
34 Catechol

## 35 1. Introduction

36 Phenolic compounds are present at low levels in subterranean and drinking waters, as a result  
37 of their wide use in textiles, plastics, dyes, paper, herbicides and pesticides (Shan et al., 2009;  
38 Lu et al., 2010, Zhao et al., 2012). As environmental pollutants, dihydroxybenzene isomers  
39 have been the subject of many studies due to their presence and difficult degradation (Wang et  
40 al., 2012). Catechol (CT, 1,2-dihydroxybenzene) is one of the most important phenolic  
41 compounds found in teas, vegetables, fruits and tobaccos. Considered as one of the key  
42 fragments of tea catechins, CT is contained in tea at various concentrations ranging from 0.1  
43 mg.g<sup>-1</sup> to 0.1 g.g<sup>-1</sup> (Montserrat et al., 2010; Li et al., 2009). Tea also contains proteins, amino  
44 acids, alkaloids, carbohydrates, lipoids, organic acids and inorganic elements. CT is of great  
45 biological importance with respect to anti-oxidant properties, antiviral and enzyme activities;  
46 however, an excessive intake may cause some health problems (Chambers, 1988; Yue et al.,  
47 2013). CT is considered as an environmental pollutant by the European Union (EU) (Xie et  
48 al., 2006). It is responsible for renal tube degeneration and liver function decrease (Aziz et al.,  
49 2007). At low concentration in foods and cigarettes, it can cause mutagenesis and cancerous  
50 alterations (Hirakawa et al., 2002). Thus, it is critical to establish highly sensitive and  
51 selective analytical tools to identify and quantify traces of catechol in environmental samples.  
52 Up to now, the most commonly used analytical methods include spectrophotometry (Nagaraja  
53 et al., 2001), gas chromatography (Moldoveanu & Kiser, 2007) and high-performance liquid  
54 chromatography (HPLC) (Marrubini et al., 2005). These techniques have some disadvantages,  
55 such as complicated operation, poor selectivity and high cost and require highly skilled  
56 manpower. Electroanalytical methods may be of interest owing to their sensitivity, rapidity,  
57 simplicity and low cost (Fekadu et al., 2013). Thus, some electrochemical methods have been  
58 developed for the sensitive detection of CT (Wang et al., 2007; Lin et al., 2009; Zhao et al.,  
59 2009, 2012; Yue et al., 2013; Yuan et al., 2013). They are mostly based on the use of  
60 chemically modified electrodes, such as anthraquinone modified carbon paste electrode  
61 (Fekadu et al., 2013), multi-walled carbon nanotube modified carbon paste electrode  
62 (Yongqing et al., 2017) and mesoporous Al-doped silica modified electrode (Lin et al., 2009).  
63 The modification of the electrode surface is intended to enhance both sensitivity and  
64 selectivity of the detection, but the above examples are based on the use of rather costly  
65 modifiers. The development of new composite materials, cheap and easy to prepare, likely to  
66 be used as effective electrode modifiers for the sensitive detection of CT is still needed.

67 Clay minerals are considered nowadays as interesting adsorbent materials due their low cost,  
68 abundance, their morphology ensuring a high surface-to-volume ratio and thus developing  
69 large active surface areas. In that context, for instance, [Kong et al. \(2011\)](#) reported a  
70 palygorskite modified carbon paste electrode for the determination of CT. However the  
71 adsorption capacities and the intrinsic selectivity of natural clays towards organic and  
72 inorganic pollutants can be low, restricting the extensive use of these materials ([Guggenheim  
73 and Martin, 1995](#)). In the aim to get more efficient adsorbents, the elaboration of organic-  
74 inorganic hybrid materials based on the chemical modification of surface properties of natural  
75 clays with organo-functional moieties has become a promising way during the past decades  
76 ([Tonle et al., 2003, 2005](#)). The so-called organoclays can be obtained by modifying clays and  
77 clay minerals with organic groups through several processes: intercalation (or insertion), ion  
78 exchange, pillaring or surface grafting ([Park et al., 2004; Piscitelli et al., 2010](#)). On the other  
79 hand, organoclay modified electrodes have been largely exploited in electroanalysis ([Tonle et  
80 al., 2015](#)), and most studies reported to date have been focused on layered clay minerals  
81 (smectite and kaolinite being the most investigated ones), which can be grafted via the  
82 hydroxyl groups localized at the outer surfaces or on the edges of clay particles (for smectite-  
83 type clays) or along the unshared plane of the alumina sheets in kaolinite.  
84 In this study, amino-functionalized montmorillonites (Mt-NH<sub>2</sub> and MtH-NH<sub>2</sub>) have been  
85 prepared by grafting [3(2-aminoethyl)]propyltrimethoxysilane (AEP-TMS) on purified clay  
86 mineral sample (Mt-Na), then on the same clay sample chemically activated in acid medium  
87 (MtH). For MtH-NH<sub>2</sub> material, the acid activation was performed before the grafting process  
88 to increase its surface area and enrich its structure with –OH binding sites ([Gonzalez et al.,  
89 1984; Rodriguez et al., 1994, Angela de Mello et al. 2009](#)). This may further result in an  
90 enhancement of the amount of grafted organosilanes. After characterization of the starting and  
91 modified clay materials, it was demonstrated that MtH-NH<sub>2</sub> can be used as prominent  
92 modifier for a GCE, and exploited for the preconcentration and sensitive detection of CT in  
93 water and tea samples.

94

## 95 **2. Experimental**

### 96 *2.1. Clay mineral, materials and chemicals*

97 The Na-montmorillonite clay mineral used in this work was obtained from the Source  
98 Clays Repository, University of Missouri-Columbia (Columbia, MO 65211, USA). The Na-  
99 montmorillonite has the chemical formula NaSi<sub>16</sub>(Al<sub>6</sub>FeMg)O<sub>20</sub>(OH)<sub>4</sub> ([Van Olphen &](#)

100 [Fritpiat, 1979](#)). All chemicals were obtained commercially and used without further  
101 purification. Catechol ( $C_6H_6O_2$ , 99%, Sigma-Aldrich),  $H_3BO_3$ (98%, Fisher Scientific  
102 International), HCl (36%, Phillip Harris),  $CH_3COOH$  (Prolabo), KCl (99.5%, Fisher Scientific  
103 International),  $H_3PO_4$ (63%, Prolabo),  $K_2HPO_4$  (99% Prolabo),  $KH_2PO_4$ (99% Prolabo),  
104 ( $CH_3COONa$ ) (99% Prolabo), Hexaammineruthenium(III) chloride ( $Ru(NH_3)_6Cl_3$ , 98%,  
105 Sigma-Aldrich), and potassium hexacyanoferrate(III) ( $K_3Fe(CN)_6$ , Fluka) served as redox  
106 probes for permeability characterization of the film modified electrodes. Various electrolytes  
107 such as acetate buffer solution (0.1 M AB), phosphate buffer solution (0.1 M PB), and  
108 Britton-Robinson buffer solution (0.1 M BRB) were prepared from the appropriate chemicals  
109 mentioned above. The grafting agent ([3-(2-Aminoethylamino)propyl]trimethoxysilane, AEP-  
110 TMS,  $\geq 98\%$ ) used for clay modification was obtained from Sigma-Aldrich. A tea sample was  
111 purchased from local market and treated as follow. Briefly, the tea sample was powdered with  
112 a mortar and a weighed portion (0.055 g) was used for catechol extraction with 50 mL of 90%  
113 ethanol/water solution for 24 h shaking at  $80^\circ C$ . The mixture was filtered and the volume  
114 made up to 25.0 mL for further measurement. All solutions were prepared with distilled water  
115 and experiments were carried out at room temperature.

## 116 *2.2. Preparation of grafted materials*

117 Before the grafting process, 1.5 g of sodium montmorillonite (Mt-Na) was activated  
118 with 150 mL of a 0.1 M HCl solution. This suspension was stirred for 4 h. Acid activation  
119 was used to remove sodium ions from the interlayer region. Then, 1 g of acid-activated  
120 montmorillonite, previously dried at  $130^\circ C$  for 4 h, was dispersed in 50 mL of 0.1 M AEP-  
121 TMS in dry toluene. The resulting mixture was heated and allowed to reflux under stirring for  
122 72 h in an inert  $N_2$  atmosphere. The solid obtained was washed successively with toluene,  
123 ethyl alcohol and then filtered. The product MtH-NH<sub>2</sub> was finally dried for 2 h at  $120^\circ C$  in an  
124 inert nitrogen atmosphere and stored in a flask. The same procedure was applied to get Mt-  
125 NH<sub>2</sub>, using the purified clay without the acid activation step.

## 126 *2.3. Preparation of the working electrodes*

127 The elaboration of sensors involved the deposition of each organoclay films onto glassy  
128 carbon electrode (GCE) surfaces by "drop coating". The GCE was first polished with alumina  
129 pastes and then rinsed for 5 min in a 1:1 water-ethanol mixture under sonication in order to  
130 remove any remaining alumina particles. Subsequently, aqueous dispersions of either raw Mt-  
131 Na, Mt-NH<sub>2</sub> or MtH-NH<sub>2</sub> (at  $5\text{ mg}\cdot\text{mL}^{-1}$ ) were prepared and 6  $\mu\text{L}$  (30  $\mu\text{g}$  of clay) were drop-

132 coated onto the top of the GCE (surface area:  $0.071 \text{ cm}^2$ ), which was dried at  $110^\circ\text{C}$  for 4 min  
133 in an oven prior to use. Throughout the text, the modified electrodes are referred to as  
134 GCE/Mt-Na, GCE/Mt-NH<sub>2</sub> and GCE/MtH-NH<sub>2</sub> for the GCE modified by raw Mt-Na, Mt-  
135 NH<sub>2</sub> and MtH-NH<sub>2</sub>, respectively.

#### 136 *2.4. Electrochemical procedures and apparatus*

137 Cyclic voltammetry, electrochemical impedance spectroscopy (EIS) and differential  
138 pulse voltammetry (DPV) measurements were performed using the palmsens<sup>3</sup> potentiostat,  
139 equipped with the PS Trace 4.2 electrochemical analysis system and connected to a computer.  
140 The voltammograms were recorded under quiescent conditions immediately after the  
141 immersion of the working electrode in a conventional single compartment cell containing the  
142 “analyte + electrolyte” solution, a pseudo reference electrode (Ag/Ag<sup>+</sup>) and a platinum wire  
143 auxiliary electrode. Differential pulse voltammetry (DPV) measurements were performed in a  
144 25 mL electrochemical cell containing 0.1 M Britton-Robinson buffer (BRB) solution (pH 4)  
145 and catechol at appropriate concentrations, in the potential range from -0.2 V to 0.8 V. All  
146 experiments were conducted at room temperature ( $25^\circ\text{C}$ ). EIS were carried out in 5 mM  
147  $[\text{Fe}(\text{CN})_6]^{3-/4-}$  (1:1) solution containing 0.1 M KCl over the frequency range of 0.1 Hz-10  
148 kHz. The morphology of modified GCEs was analyzed by scanning electron microscopy  
149 (SEM) using a JEOL JCM-6000 apparatus (acceleration voltage of 15 kV). Fourier transform  
150 infrared spectroscopy (FTIR) was applied to assess the presence of organic groups in the final  
151 materials, using a Nicolet 8700 apparatus equipped with a specular reflectance accessory  
152 (Smart Collector). The crystallinity of raw and modified clay materials was determined by X-  
153 ray diffraction analysis using a Stoe Stadi-p X-ray powder diffractometer (Stoe & Cie GmbH,  
154 Darmstadt, Germany), with Cu K $\alpha$ 1 radiation (40 kV, 30 mA and  $\lambda_{\text{Cu}}=1.54056 \text{ \AA}$ ). The  
155 Brunauer-Emmett-Teller (BET) surface areas of the samples were determined by means of  
156 N<sub>2</sub> adsorption at 77.13 K using a micrometrics model sorptometer (Thermo Electron  
157 Corporation, Sorptomatic Advanced Data Processing). Before N<sub>2</sub> adsorption, the samples  
158 were degassed at 307.13 K under vacuum. The surface area was defined from linear part of  
159 the BET equation. CHN elemental analysis was performed using CHNS Analyzer Euro EA  
160 3000. The thermal behavior of the clay mineral before and after its modification was  
161 investigated by the thermogravimetric analysis (STA 409 C equipment Netzsch Geratebau  
162 GmbH, Germany). Approximately 10 mg of each dried sample were heated from 25 to 1000  
163 °C under nitrogen atmosphere with a heating rate of 10 °C/min. The pH of solutions was  
164 monitored using an Inolab pH-meter.

### 165 3. Results and discussion

#### 166 3.1. Physico-chemical characterization of composite materials

167 FTIR spectroscopy was used to identify and compare the functional groups present in natural  
168 montmorillonite (Mt-Na), acid treated Mt (MtH) and modified montmorillonite (Mt-NH<sub>2</sub> and  
169 MtH-NH<sub>2</sub>) as shown in Fig. 1. On the spectrum of raw clay mineral (Fig. 1a), one can observe  
170 a stretching vibration band at 3620 cm<sup>-1</sup>, which is characteristic of Al-OH stretching of the  
171 octahedral sites of natural montmorillonite (Biernacka, 2005), while the bending mode of  
172 such hydroxyl groups appears at 916 cm<sup>-1</sup> (Qin et al., 2010). The peaks observed at 3404 and 1640  
173 cm<sup>-1</sup> are attributed to the -OH stretching and bending vibrations of physisorbed water in the  
174 interlamellar space of montmorillonite, respectively. Others observed bands, appearing on all  
175 investigated materials between 700 and 450 cm<sup>-1</sup> correspond to Si-O-Si stretching (690 cm<sup>-1</sup>)  
176 and deformation (516 and 468 cm<sup>-1</sup>) of tetrahedral sites (Mendelovici, 1973). The signals at  
177 885, 843 and 777 cm<sup>-1</sup> are due to Al-OH deformation, Fe-OH deformation and Mg-OH  
178 deformation respectively (Amarasinghe et al., 2008; Katti et al., 2006). After acid activation,  
179 some changes in the FTIR spectra (Fig. 1b) can be observed. The band intensity at 3620 and  
180 1640 cm<sup>-1</sup> increased slightly, thus suggesting that the MtH sample is more hydrophilic than  
181 the Mt-Na. The appearance of a shoulder around 3150 cm<sup>-1</sup> traduces the presence of Si-OH  
182 groups arising upon Si-O-Al bonds breaking during the acid pretreatment. The OH stretching  
183 region of Mt is sensitive to the effects of interlayer modification, and the intercalation  
184 followed by the grafting of the organosilane on the internal surface -OH groups of MtH  
185 should have a major influence on the OH stretching pattern of the grafted organoclays. As a  
186 matter of fact, upon grafting of AEP-TMS, some pronounced changes occurred in the spectra  
187 of amino-montmorillonite clays samples (Mt-NH<sub>2</sub> and MtH-NH<sub>2</sub>) (Fig. 1c and 1d): the new  
188 absorption band at 2928 cm<sup>-1</sup> is due to the antisymmetric stretching of -CH<sub>2</sub> bonds (Qin et al.,  
189 2010, Xue et al., 2011, ) while the bands appearing at 1473 cm<sup>-1</sup> and 1316 cm<sup>-1</sup> are assigned to  
190 -CH<sub>2</sub>- scissoring deformation (symmetric and asymmetric respectively), both from the silane  
191 coupling agent. The symmetric stretching of -CH<sub>2</sub> bonds are also visible at 2840 cm<sup>-1</sup> (Qin et  
192 al., 2010). Comparing curves (c) & (d) of Figure 1 enables to point out qualitatively the  
193 interest of the acidic treatment on the efficiency of the functionalization (slightly more intense  
194 C-H bond for the MtH-NH<sub>2</sub> sample). The grafting process leads to a decrease in the intensity  
195 of the bands characteristics of OH stretching and bending vibrations of adsorbed water and  
196 the hydroxyl groups (respectively at 3404 and 1640 cm<sup>-1</sup>) and a very small deviation of the  
197 positions of these bands. This is due in one hand to the involvement of the hydroxyl groups in

198 the grafting process, and in another hand to the removal of cations from the octahedral layer  
199 which causes some loss of water molecules.

200

201

**(Figure 1 near here)**

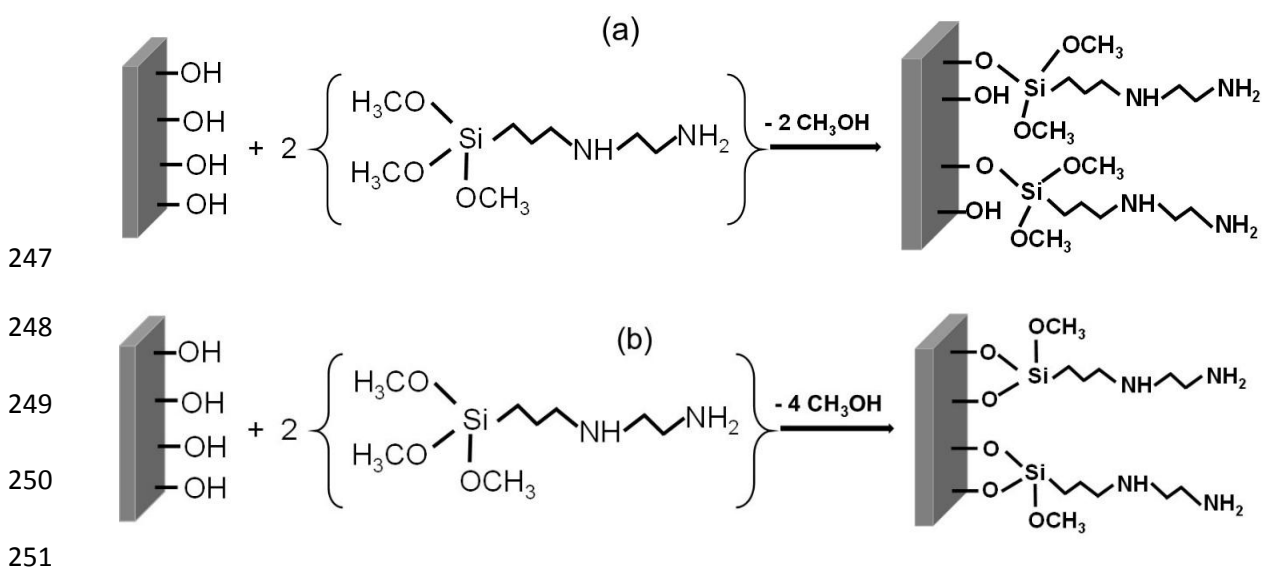
202 XRD patterns of raw Mt-Na, acid treated Mt (MtH), Mt-NH<sub>2</sub> and MtH-NH<sub>2</sub> are shown in Fig.  
203 2. A comparison of the results obtained indicates that the original structure has been retained  
204 after modification. An approximate value of 1.21 nm ( $2\theta = 7.3^\circ$ ) was estimated for the basal  
205 spacing  $d_{001}$  of the Mt-Na sample (Fig. 2A, curve a). The acid activation led to an increase in  
206 the basal spacing (1.21 to 1.30 nm), most likely due to water adsorption. The increased  
207 hydrophilic feature of the MtH (Fig. 2A, curve b) with respect to the starting Mt was  
208 previously indicated by the IR results. Direct grafting of AEP-TMS onto Mt-Na showed a  
209 minimal difference in basal spacing between the Mt-Na and Mt-NH<sub>2</sub> samples (1.21 nm to 1.36  
210 nm at  $2\theta = 6.5^\circ$ ) (Fig. 2A, curve c). This slight difference is probably due to a small amount  
211 of AEP-TMS in the interlamellar space of the clay mineral. Usually, the intercalation of guest  
212 species in montmorillonite layers induces significant changes in the basal spacing (Mercier &  
213 Detellier, 1995). The acid activation used in MtH-NH<sub>2</sub> synthesis resulted in a much bigger  
214 increase in the basal spacing of the MtH and MtH-NH<sub>2</sub> samples (1.30 nm to 1.80 nm) (Fig.  
215 2A, curve c), probably due to AEP-TMS incorporated in basal spacing. It may indicate that  
216 the silane molecules were mainly hydrolyzed and condensed with the hydroxyl groups on the  
217 external surface of Mt. Another explanation could be that the interlayer organosilane  
218 molecules were hydrolyzed and condensed to form a cross-linked structure, causing small  
219 increase on the basal spacing and influencing the grafting of AEP-TMS on MtH. The TGA  
220 curves (Fig. 2B) revealed a significant increase in the loss of adsorbed water mass on the MtH  
221 (Fig. 2B, curve b) compared to raw Mt (Fig. 2B, curve a). Usually, the increase in water  
222 content leads to an increase in the basal spacing. This increase in water molecules is explained  
223 by the replacement of sodium ions in the interlayer space by water molecules. On the  
224 materials Mt-NH<sub>2</sub> (Fig. 2B, curve c) and MtH-NH<sub>2</sub> (Fig. 2B, curve d), the mass losses of  
225 absorbed water are comparable to that of the raw clay. Our hypothesis is that for the Mt-NH<sub>2</sub>  
226 sample, the organosilane was grafted on the surface without replacement of sodium ions while  
227 for the MtH-NH<sub>2</sub>, there was replacement of water molecules in the interlayer space of MtH  
228 and grafting on the surface.

229

230

(Figure 2 near here)

231 Elemental analysis was performed on the amino-grafted materials (Mt-NH<sub>2</sub> and MtH-NH<sub>2</sub>)  
 232 for C, H and N. The results obtained were 11.07 % C, 2.60 % H, 4.66 % N for Mt-NH<sub>2</sub> and  
 233 9.73 % C, 2.44 % H, 3.89 % N for MtH-NH<sub>2</sub>. This was evidence of the presence of nitrogen-  
 234 containing moieties. To determine the structural formula of the grafted clay using the the  
 235 chemical formula of Mt, NaSi<sub>16</sub>(Al<sub>6</sub>FeMg)O<sub>20</sub>(OH)<sub>4</sub>, we assumed grafting via one, two, three  
 236 or four methoxy groups on one clay mineral structural unit as usually obtained during  
 237 silylation of montmorillonite surfaces (Su et al., 2012). The theoretical content of C: 11.34%,  
 238 H: 2.72%, N: 3.78% for Mt-NH<sub>2</sub> and 10.04 % C, 2.46 % H, 3.90 % N for MtH-NH<sub>2</sub> is in  
 239 accordance with the mechanism proposed in Scheme 1, supporting the idea that the chemical  
 240 bonding of AEP-TMS on the clay material was effective as revealed by infrared results. The  
 241 proposed structural formulas of Mt-NH<sub>2</sub> and MtH-NH<sub>2</sub> were  
 242 NaSi<sub>16</sub>(Al<sub>6</sub>FeMg)O<sub>20</sub>(OH)<sub>2</sub>[OSi(OCH<sub>3</sub>)<sub>2</sub>(CH<sub>2</sub>)<sub>3</sub>NH(CH<sub>2</sub>)<sub>2</sub>NH<sub>2</sub>]<sub>2</sub> and  
 243 Si<sub>16</sub>(Al<sub>5</sub>FeMg)O<sub>21</sub>(OH)<sub>3</sub>[O<sub>2</sub>Si(OCH<sub>3</sub>)(CH<sub>2</sub>)<sub>3</sub>NH(CH<sub>2</sub>)<sub>2</sub>NH<sub>2</sub>]<sub>2</sub> respectively. An increase in Si-  
 244 OHs bonds and a decrease in the number of Al can be observed in the MtH-NH<sub>2</sub> formula  
 245 compared to Mt-NH<sub>2</sub> formula. These increase and decrease occurred during the acid  
 246 pretreatment by Si-O-Al bonds breaking during the removal of Al.



252 **Scheme 1.** Proposed mechanism for the grafting of AEP-TMS on (a) Mt and (b) MtH.

253 The sodium montmorillonite clay sample is mesoporous with a specific surface area of 31.48  
 254 m<sup>2</sup>/g. After direct grafting, the specific surface area of the synthesized material (Mt-NH<sub>2</sub>)  
 255 decreased to 8.49 m<sup>2</sup>/g, suggesting that the organosilane is covalently bound to the individual

256 -OH groups at the edge of clay platelets, as shown by a previous work (Celis et al., 2000). It is  
257 known that the low silanol surface density of montmorillonite clay mineral is a main factor  
258 limiting the covalent grafting of organic ligands and that better performance can be obtained  
259 by grafting organic functions in the interlayer region of montmorillonite (Celis et al., 2000;  
260 Mercier and Detellier, 1995). Another sample of sodium montmorillonite was activated in  
261 acid medium (MtH) and then functionalized (MtH-NH<sub>2</sub>). A specific surface area of 19.66  
262 m<sup>2</sup>/g obtained for the MtH-NH<sub>2</sub> material suggests a low graft rate on the surface of the  
263 material but the increase in basal spacing obtained in XRD analysis from 1.36 nm (Mt-NH<sub>2</sub>)  
264 to 1.80 nm (MtH-NH<sub>2</sub>) confirms the intercalation followed by the concomitant coupling of the  
265 organosilane moieties on the -OH groups found the internal surface of on the clay layers, and  
266 on the borders of the clay platelets.

267 SEM micrographs of the GCE modified in turn by Mt-Na, acid treated Mt (MtH), Mt-NH<sub>2</sub>  
268 and MtH-NH<sub>2</sub> respectively are shown in Fig. 3. On the micrographs of GCE/Mt-Na and  
269 GCE/MtH (Fig. 3a & 3b), one can observe the strong tendency toward aggregation and the  
270 compact aspect of the material, with particles arranged in the form of agglomerates of  
271 irregular shape and flat surface. For the Mt-NH<sub>2</sub> and MtH-NH<sub>2</sub> modified GCEs (Fig. 3c & 3d),  
272 the particles are even more agglomerated and present onto the electrode surface as big  
273 aggregates, suggesting that the functionalization of clay may have contributed to enhance the  
274 edge-to-edge and face-to face interactions between organoclay platelets.

275

276 **(Figure 3 near here)**

277

### 278 *3.2. Permeability properties of various modified electrodes*

279 The electrochemical behavior of redox species at clay modified electrodes is expected to be  
280 affected by three main parameters: the concentration of the analyte, the accessible area of the  
281 working electrode and the speed of mass transfer for the probe within the film (Fitch, 1990).  
282 Cyclic voltammetry (CV) was applied to the modified electrodes to evaluate their  
283 preconcentration/rejection properties or permselective behavior towards [Fe(CN)<sub>6</sub>]<sup>3-</sup> and  
284 [Ru(NH<sub>3</sub>)<sub>6</sub>]<sup>3+</sup> electroactive probes. CV experiments were performed using the bare GCE,  
285 GCE/Mt-Na, GCE/Mt-NH<sub>2</sub> and GCE/MtH-NH<sub>2</sub> in 0.1 M KCl/HCl solution at pH 1. Both  
286 probes gave rise to well defined reversible CV responses at on the bare GCE (curves (a) in  
287 Figure 4(A) & (B)). The peak current values obtained are I<sub>pa</sub> 3.06 μA (anodic), I<sub>pc</sub> 2.9 μA

288 (cathodic) and  $I_{pa}$  1.46  $\mu\text{A}$  (anodic),  $I_{pc}$  1.95  $\mu\text{A}$  (cathodic), respectively for  $[\text{Fe}(\text{CN})_6]^{3-}$  and  
289  $[\text{Ru}(\text{NH}_3)_6]^{3+}$  probes, and they did not change upon multiple potential scanning. This was not  
290 the case when recording multisweep CV curves at the clay-modified electrodes. Typical  
291 results obtained for 0.5 mM  $[\text{Fe}(\text{CN})_6]^{3-}$  probe (in the potential range of 0.0 V to 0.6 V) are  
292 illustrated in Fig. S1 (Supplementary data). On Fig. S1a, one can see that the voltammetric  
293 signal on the GCE/Mt-Na is constant over multiple potential scans, the peak currents values  
294 ( $I_{pa}$  1.30  $\mu\text{A}$ ,  $I_{pc}$  1.27  $\mu\text{A}$ ) lower than those obtained at the bare. Such behavior is explained  
295 by the electrostatic repulsions between the negative surfaces of Mt-Na and the anionic probe  
296  $[\text{Fe}(\text{CN})_6]^{3-}$  (Tonle et al., 2004). On the opposite, CV signals were found to grow dramatically  
297 upon multisweep scan when using the amino-montmorillonite modified GCE (Fig. S1 b & c),  
298 indicating the progressive accumulation of  $[\text{Fe}(\text{CN})_6]^{3-}$  that leveled off after about 50 scans,  
299 with steady-state peak current values larger by one order of magnitude than on bare GCE  
300 (Fig. 4A). Such accumulation is due to the electrostatic attraction between the negative redox  
301 probe  $[\text{Fe}(\text{CN})_6]^{3-}$  and the positively charged amino groups present in the AEP-TMS chain  
302 grafted onto the montmorillonite surface (which are protonated in the acidic analysis medium  
303 used here, in the form of  $-\text{NH}_3^+$  groups). As also shown in Fig. 4A, the electrochemical signal  
304 after 50 scans on GCE/MtH-NH<sub>2</sub> ( $I_{pa}$  22.22  $\mu\text{A}$ ,  $I_{pc}$  23.66  $\mu\text{A}$ ) is significantly higher than  
305 those obtained on GCE/Mt-NH<sub>2</sub> ( $I_{pa}$  14.79  $\mu\text{A}$ ,  $I_{pc}$  17.74  $\mu\text{A}$ ). This difference is due to a  
306 larger content of AEP-TMS groups grafted onto the acid-treated montmorillonite.

307 Cyclic voltammetry of cationic probe  $[\text{Ru}(\text{NH}_3)_6]^{3+}$  (Fig. S2 in Supplementary data) was also  
308 carried out in the potential range of -0.5 V to 0.0 V in the same electrolyte solution as above  
309 (0.1 M KCl/HCl, pH 1). For GCE coated with Mt-Na, a progressive accumulation was  
310 observed, reaching steady-state current values after about 50 scans (Fig. S2a). The peak  
311 currents at saturation ( $I_{pa}$  19.33  $\mu\text{A}$ ,  $I_{pc}$  18.06  $\mu\text{A}$ ) were much larger than those obtained at  
312 the bare GCE ( $I_{pa}$  1.46  $\mu\text{A}$ ,  $I_{pc}$  1.95  $\mu\text{A}$ ), as explained by favorable electrostatic attraction  
313 between the cationic redox probe and the negatively charged montmorillonite platelets. This  
314 behavior results from both true physical diffusion of the analyte upon ion exchange in the  
315 coating, and mass-charge transfer phenomena arising from potential scanning (Tonle et al.,  
316 2004). On the opposite, when using GCE/Mt-NH<sub>2</sub> and GCE/MtH-NH<sub>2</sub> in the same conditions  
317 (Fig. S2 b & c), the protonated organoclay films acted as electrostatic barrier preventing the  
318 uptake of the cationic  $[\text{Ru}(\text{NH}_3)_6]^{3+}$  species. This resulted in much lower redox peak currents  
319 on GCE/Mt-NH<sub>2</sub> ( $I_{pa}$  3.81  $\mu\text{A}$ ,  $I_{pc}$  4.81  $\mu\text{A}$ ) and GCE/MtH-NH<sub>2</sub> ( $I_{pa}$  2.21  $\mu\text{A}$ ,  $I_{pc}$  3.62  $\mu\text{A}$ )  
320 than for the non-grafted clay film electrode GCE/Mt-Na (Fig. 4B), as explained by the  
321 electrostatic repulsions between the positively charged redox probe and the  $-\text{NH}_3^+$  groups of

322 the organoclays. Again, the permselective effect was more intense for GCE/MtH-NH<sub>2</sub>  
323 electrode, supporting the idea that acid activation prior to AEP-TMS grafting resulted in more  
324 effective montmorillonite modification.

325 **(Figure 4 near here)**

### 326 3.3. EIS results

327 Electrochemical impedance spectroscopy (EIS) was used to evaluate the electrochemical  
328 properties of the various electrodes. In EIS, the semicircle portion at higher frequencies  
329 corresponds to the electron-transfer limited process (equals the charge-transfer resistance,  
330  $R_{ct}$ ), and the linear part at lower frequencies corresponds to the diffusion process. Fig. 5  
331 shows the Nyquist plots of EIS for the bare GCE, GCE/Mt-Na, GCE/Mt-NH<sub>2</sub> and GCE/MtH-  
332 NH<sub>2</sub> electrodes, as recorded in 0.1 M KCl containing 5 mM  $[\text{Fe}(\text{CN})_6]^{3-/4-}$  (1:1) solution over  
333 the frequency range of 0.1 Hz-10 kHz. At the bare GCE (curve (a) in Fig. 5), the probe is easy  
334 to transfer electron on the electrode surface, yet with a non-negligible  $R_{ct}$  value of 4736  $\Omega$ .  
335 The charge-transfer resistance was even larger ( $R_{ct} = 5263 \Omega$ ) when using GCE/Mt-Na (curve  
336 (b) in Fig. 5), which is explained by some shielding behavior of the positively charged Mt  
337 clay particles on the anionic  $[\text{Fe}(\text{CN})_6]^{3-/4-}$  species. With the grafting of AEP-TMS on Mt-Na,  
338 the resistance decreased (see curves (c) and (d) of Fig. 5), implying that Mt-NH<sub>2</sub> and MtH-  
339 NH<sub>2</sub> promote the transport properties of the  $[\text{Fe}(\text{CN})_6]^{3-/4-}$  probes. This resulted in lower  $R_{ct}$   
340 values ( $R_{ct} = 114.35 \Omega$  with GCE/MtH-NH<sub>2</sub> and  $R_{ct} = 167.84 \Omega$  with GCE/Mt-NH<sub>2</sub>), the small  
341 difference between them being again due to the fact that acid activation allowed the binding  
342 of a greater amount of AEP-TMS moieties on the Mt clay.

343 **(Figure 5 near here)**

344

### 345 3.4. Preliminary studies on the electrochemical behavior of catechol

#### 346 3.4.1. Direct electrochemistry of catechol

347 The electrochemical behaviour of catechol on various electrodes was carried out in 0.1 M  
348 Britton-Robinson buffer (BRB) solution at pH 4 in the potential range from -0.2 V to 0.8 V,  
349 and the results are shown in Fig. 6. A pair of quasi-reversible redox peaks are observed on all  
350 CV curves, indicating that the electroactive substance can reach and be detected on all  
351 electrode surfaces. Nevertheless, significant variations in peak intensity were observed

352 depending on the electrode type. Peak currents were almost 2-fold lower on GCE/Mt-Nathan  
353 on bare GCE (curves(a) & (b) on Fig. 6), whereas significantly more intense signals were  
354 observed when passing to GCE modified by amino-grafted materials (curves(c) & (d) on Fig.  
355 6). This indicates the interest of the amino-grafted materials for enhancing the CT oxidation  
356 signal, suggesting the existence of accumulation effects originating from the grafted material,  
357 which are likely to improve the detection of CT, yet with slightly better response for  
358 GCE/MtH-NH<sub>2</sub> than for GCE/Mt-NH<sub>2</sub> (compare curves (c) & (d) on Fig. 6). This  
359 demonstrates the interest of the acid activation used during the grafted process to prepare  
360 MtH-NH<sub>2</sub> material, and also for CT detection. Such improvement is similar to that observed  
361 for the negatively charged redox probe discussed above (Fig. 4A), but in the present case  
362 “simple” electrostatic considerations cannot explain the phenomenon as catechol is neutral at  
363 pH values below its pKa (9.14) (Nurchi et al., 2009), and deprotonated at pH above that pKa.  
364 The CV results indicate a clear positive effect of the ethylenediamino groups grafted on the  
365 clay material, and this was also confirmed for CT detection by DPV (see section 3.5.1). A  
366 possible explanation could be a favoured incorporation of CT in the organoclay as a result of  
367 larger interlayer distance between the clay sheets upon grafting (see section 3.1 and Fig. 2)  
368 and also a more hydrophobic environment generated by the acidic treatment (in comparison  
369 to the hydrophilic Mt-Na material). The O and N groups of Mt-NH<sub>2</sub> and MtH-NH<sub>2</sub> acted as  
370 electron transfer mediators by possibly forming hydrogen bonding interactions with hydroxyl  
371 groups of CT. They have contributed to weakening the hydroxyl bond energies and facilitated  
372 the electron transfer through O- -HO and N- -HO (Ding et al., 2005).  
373 The Mt-NH<sub>2</sub> and MtH-NH<sub>2</sub> modifiers might also contribute to accelerate the electron transfer  
374 rates for catechol oxidation, as suggested from slightly lower overpotentials with respect to  
375 bare GCE (compare peak potentials of curves c & d to curve a in Fig. 6), also in agreement  
376 with the much lower charge transfer resistance values observed by EIS for the modified  
377 electrodes (see section 3.3). Due to its better performance with respect to CT detection, the  
378 GCE/MtH-NH<sub>2</sub> electrode was used for further experiments.

379

380

**(Figure 6 near here)**

381

382 *3.4.2. Effect of scan rate on the electrochemical response of catechol at GCE/MtH-NH<sub>2</sub>*

383 The influence of potential scan rate on the electrochemical response of catechol was studied  
384 by cyclic voltammetry and the results obtained are shown in Fig. 7. The peak currents  
385 increased with the scan rate in the studied range (Fig. 7a), remaining linear with the square  
386 root of the scan rate ( $v^{1/2}$ ) (Fig. 7b). This indicates a diffusion-controlled process,  
387 phenomenon that was also confirmed by plotting the double logarithmic of  $I_{pa}$  vs scan rate  
388 (Fig. 7c), giving a slope ( $\partial \log(I_{pa})/\partial \log(v)$ ) equal to 0.49, close to 0.5, the characteristic value  
389 for a diffusion-controlled electron-transfer mechanism (Shih et al., 2004).

390

391

(Figure 7 near here)

392

### 393 3.5. Differential pulse voltammetry study

#### 394 3.5.1. Importance of the modification of Mt and effect of the detection medium

395 In order to evaluate the ability of AEP-TMS grafted Mt to accumulate quantitatively CT and  
396 the interest of the acid activation step before grafting, DPVs of 0.1 mM CT were recorded in  
397 0.1 M BRB solution (pH 4) on bare GCE, GCE/Mt-Na, GCE/Mt-NH<sub>2</sub> and GCE/MtH-NH<sub>2</sub>  
398 (Fig. 8). Peak currents were found to decrease from the bare GCE (1.7  $\mu$ A) to GCE/Mt-Na  
399 (0.75  $\mu$ A), and increase when passing from GCE/Mt-Na (0.75  $\mu$ A) to GCE/Mt-NH<sub>2</sub> (2.15  $\mu$ A)  
400 and to GCE/MtH-NH<sub>2</sub> (2.9  $\mu$ A). Meanwhile, the peak potentials shifted towards less anodic  
401 values: from +0.358 V on bare GCE to +0.271 V on GCE/Mt-Na, to +0.270 V on GCE/Mt-  
402 NH<sub>2</sub> and to +0.260 V on GCE/MtH-NH<sub>2</sub>. This indicates an the ability of Mt-NH<sub>2</sub> and MtH-  
403 NH<sub>2</sub> to induce effective enhancement of CT oxidation signal and improve the electron transfer  
404 rates, confirming the existence of both accumulation and electrocatalytic effects as suggested  
405 above, originating from the organoclay materials with respect to the detection of CT. Note  
406 that acid activation improved somewhat further the electrochemical detection of CT by  
407 increasing the current peak signal.

408

409

(Figure 8 near here)

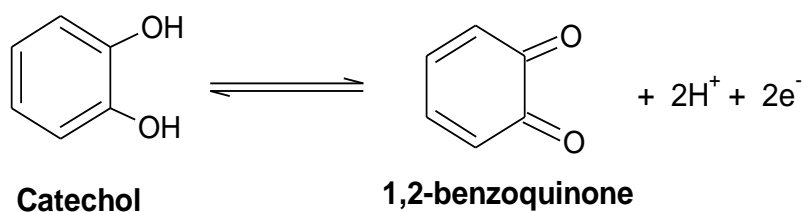
410

411 Some optimization studies were also performed. Although the composition of the detection  
412 medium was not really critical (on the basis of three different buffer solutions), the BRB  
413 solution (pH 4) was found to be more sensitive to CT detection (see Fig. S3, Supplementary

414 data). It will be thus used for further experiments. Fig. S4 (Supplementary data) shows the  
415 dependence of DPV peak currents on the accumulation time for the analysis of 0.1 mM CT at  
416 GCE/MtH-NH<sub>2</sub> electrode. The response was very fast, and the electrode was saturated after  
417 30 s, reaching a plateau up to 140 s preconcentration. Fast adsorptive equilibrium is probably  
418 due to low resistance to mass transport in such highly porous film electrode. A duration of 30  
419 s was used afterwards for the accumulation of CT.

### 420 3.5.2. Influence of pH on the peak current and potential

421 The influence of the pH of the detection medium on the electrochemical response of CT was  
422 studied in the range from 2 to 8 in BRB solution. Fig. 9a and curve (2) on Fig. 9b show that  
423 the oxidation peak potentials of CT on GCE/MtH-NH<sub>2</sub> shifted negatively with an increase in  
424 the solution pH, indicating that protons are involved in the reaction process at the electrode  
425 surface. The linear regression equation was  $E_p(\text{V}) = -0.0521 \text{ pH} + 0.4819$  ( $R^2 = 0.998$ ),  
426 demonstrating that equal number of electrons and protons are involved in the oxidation of CT.  
427 This is in agreement with the previously reported mechanism for CT, that is oxidized to 1,2-  
428 benzoquinone (Scheme 2) (Temerk et al., 2006; Unnikrishnan et al., 2012; Yue et al., 2013).  
429 Curve (1) on Fig. 9b shows the variation of the peak current of CT with pH. The peak  
430 intensity was high in acidic media, for pH values below 5, with a maximum at pH 2. The  
431 electrode response became less pronounced in basic media. The preconcentration of CT was  
432 more effective in acidic media on GCE/MtH-NH<sub>2</sub>, a BRB solution at pH 2 was used in further  
433 experiments.



434  
435 **Scheme 2.** Mechanism of catechol oxidation

436  
437 **(Figure 9 near here)**

438  
439

### 440 3.5.3. Calibration

441 The calibration graph for CT detection was plotted from DPV analyses performed under the  
442 optimal conditions obtained above, in the concentration range from 5  $\mu\text{M}$  to 80  $\mu\text{M}$ , using the  
443 GCE/MtH-NH<sub>2</sub> electrode. As shown by the inset in Fig. 10, a linear variation of peak current  
444 ( $I_p$ ) vs CT concentration was obtained in the explored range, with a sensitivity of 0.0468  
445  $\mu\text{A}\cdot\mu\text{M}^{-1}$  and a correlation coefficient of 0.999. The detection limit, defined by the relation  
446  $3S_b/m$  (where  $S_b$  represents the standard deviation on the blank and  $m$  the slope on the  
447 calibration graph) as the analyte concentration yielding such smallest detectable signal  
448 (Ghoneim et al., 2000) was estimated to 0.65  $\mu\text{M}$ . This demonstrates that GCE/MtH-NH<sub>2</sub> can  
449 be exploited for the electroanalysis of CT in aqueous media in the  $\mu\text{M}$  range. The analytical  
450 performance of GCE/MtH-NH<sub>2</sub> electrode is comparable or better than some data reported in  
451 previous literature as shown in Table 1. A relative standard deviation (RSD) of 3.1 % for  
452 parallel detections of 0.1 mM CT using five distinct electrodes (see Fig. S5 in Supplementary  
453 data) was obtained, indicating a good reproducibility and repeatability of the modified  
454 electrode. The anodic peak current of CT lost 4.6 % of its initial value, after 5 consecutive  
455 DPV measurements on the same electrode and in the same conditions. This result shows that  
456 the proposed electrode is mechanical stable and reliable for the determination of CT. The  
457 performance of the method proposed herein is comparable, and even better than some data  
458 already reported on the quantification of CT using other modified electrodes (Figueiredo et  
459 al., 2007; Sun et al., 2008; Li et al., 2009; Zhu et al., 2009).

460

461 **(Figure 10 near here)**

462 **(Table 1 near here)**

### 463 *3.6. Interference of some organic molecules and real samples analysis*

464 The effect of potential interfering molecules including hydroquinone, ascorbic acid,  
465 dopamine, citric acid, uric acid, D-glucose and quercetin on the DPVs response of CT has  
466 been studied. The results obtained are presented in Table 2. The tolerance limit was defined as  
467 the concentration ratio of the additive over CT causing less than 5.0 % relative error. Each  
468 interfering species was added in the supporting electrolyte in a concentration 5-fold higher  
469 than CT concentration. The results obtained showed that the oxidation peak of CT is greatly  
470 affected by the presence of hydroquinone, ascorbic acid and quercetin. Catechol and  
471 hydroquinone are two isomers of phenolic compounds. The broad DPV response obtained at  
472 the GCE/MtH-NH<sub>2</sub> indicated a very tiny sign of multiple components that were not easily

473 separated. However, the selectivity of the proposed sensor was evidenced by the neglected  
474 responses toward interfering species, by considering the tolerance limit defined earlier.

475

476

(Table 2 near here)

477

478 The proposed method was applied to the determination of CT in one tea sample. In this  
479 experiment, the concentration of CT was calculated using the standard addition method. The  
480 concentration of CT in tea sample was  $0.851 \text{ mg.g}^{-1}$ . The detection of CT was also evaluated  
481 for the analysis of tap and lake water samples after filtering with a Whatman paper (diameter:  
482 125mm). In DPV, no signal of CT was detected in the natural (non-spiked) water samples  
483 when using GCE/MtH-NH<sub>2</sub>, indicating that their CT contents were below the detection limit  
484 ( $0.65 \text{ }\mu\text{M}$ ). Therefore, recovery experiments were performed by measuring the DPV  
485 responses from samples to which known concentrations of CT were added. The quantitative  
486 results are summarized in Table 3. Recovery percentages of more than 110% obtained in the  
487 case of lake water are due to intensive agricultural activities around the lake where other  
488 organic compounds are found upon leaching. Yet, the amino groups on the organoclay has  
489 high affinity with many biomolecules, a fact that could explain such a result.

490

(Table 3 near here)

#### 491 4. Conclusion

492 The aim of this work was to develop a voltammetric sensor based on amino-montmorillonite  
493 and apply it to the detection of catechol. [3(2-aminoethyl)]propyl groups were grafted onto  
494 the surface of Na-montmorillonite and acid-activated montmorillonite clays. The results of the  
495 analyses by infrared spectroscopy, X-ray diffraction and EIS confirmed the effectiveness of  
496 the grafting process. It was demonstrated by CV and DPV that the detection of CT is  
497 improved when using the aminated montmorillonite (MtH-NH<sub>2</sub>) obtained after acid  
498 activation, in comparison to the bare glassy carbon electrode. With DPV, the peak current of  
499 GCE/MtH-NH<sub>2</sub> was 1.71-fold greater than signal obtained on the bare GCE. After  
500 optimization of the factors affecting the accumulation/detection steps, the proposed method  
501 was applied to the detection of catechol in real water samples and in a commercial tea sample.

502

503 **Acknowledgments**

504 Financial support from UNESCO and The World Academy of Sciences for the Advancement  
505 of Science in Developing Countries (RGA 19-257 RG/CHE/AF/AC\_G-FR3240310134  
506 awarded to I.K. Tonle) is gratefully acknowledged. A.T. Kamdem (Dr. A. Osorio Group,  
507 University of Freiburg, Germany) and G. Doungmo (Prof Dr H. Terraschke Group, Christian-  
508 Albrechts-Universität zu Kiel, Germany) are thanked for facilitation in samples analyses.

509

510 **References**

- 511 Amarasinghe, P.M., Katti, K.S., Katti, D.R., 2008. Molecular hydraulic properties of montmorillonite:  
512 a polarized Fourier transform infrared spectroscopic study. *Appl. Spectrosc.* 62(12), 1303-1313.
- 513 Angela de Mello F.G., Virginia S.T.C., Wander L.V., 2009. Smectite organofunctionalized with thiol  
514 groups for adsorption of heavy metal ions. *Appl. Clay Sc.* 42, 410-414.
- 515 Aziz, M.A., Selvaraju, T., Yang, H., 2007. Selective determination of catechol in the presence of  
516 hydroquinone at bare indium tin oxide electrodes via peak-potential separation and redox  
517 cycling by hydrazine. *Electroanalysis* 19, 1543-1546.
- 518 Biernacka, K.I., Silva, A.R., Carvalho, A. P., Pires, J., Freire, C., 2005. Organo-laponites as novel  
519 mesoporous supports for Manganese(III) salen catalysts. *Langmuir* 21(23), 10825-10834.
- 520 Celis, R., Hermosin, M.C., Cornejo, J., 2000. Heavy metal adsorption by functionalized clays.  
521 *Environ. Sci. Technol.* 34, 4593-4599.
- 522 Chambers, J.Q., (Eds.), 1988. The Chemistry of quinonoid compounds, in: S. Patai, Z. R. (Eds.),  
523 Wiley & Sons, volume 2, New York, pp 719.
- 524 Ding, Y.P., Liu, W.-L., Wu, Q.-S., Wang, X. G., 2005. Direct simultaneous determination of  
525 dihydroxybenzene isomers at C-nanotube-modified electrodes by derivative voltammetry. *J.*  
526 *Electroanal. Chem.* 575, 275-280.
- 527 Fekadu, M., Mesfin, R., Merid, T., Esayas, A., 2013. Electrochemical determination of catechol in tea  
528 samples using anthraquinone modified carbon paste electrode. *Nat. Sci.* 5(8), 888-894.
- 529 Figueiredo, E.C., Tarley, C.R.T., Kubota, L.T., Rath, S., Arrud, M.A.Z., 2007. Online molecularly  
530 imprinted solid phase extraction for the selective spectrophotometric determination of catechol.  
531 *Microchem. J.* 85, 290-296.
- 532 Fitch, A., 1990. Clay-modified electrodes: a review, *Clays Clay Miner.* 38, 391-400.
- 533 Gaber, A.M.M., 2009. Electrochemical sensor for voltammetric determination of catechol based on  
534 screen printed graphite electrode. *Int. J. Elechem. Sci.* 4, 1167-1177.
- 535 Ghoneim, M.M., Hassanein, A.M., Hammam, E., Beltagi, A.M., 2000. Simultaneous determination of  
536 Cd, Pb Cu, Sb, Bi, Se, Zn, Mn, Ni, Co and Fe in water samples by differential pulse stripping  
537 voltammetry at a hanging mercury drop electrode. *Fresenius J. Anal. Chem.* 367, 378-383.

538 Guggenheim, S., Martin, R.T., 1995. Definition of clays and clay minerals: Joint of AIPEA and CMS  
539 nomenclature Committees. *Clay Miner.* 30(3), 257-259.

540 Hirakawa, K., Oikawa, S., Hiraku, Y., Hirose, I., Kawanishi, S., 2002. Catechol and hydroquinone  
541 have different redox properties responsible for their differential DNA-damaging ability. *Chem.*  
542 *Res. Toxicol.* 15, 76-82.

543 Katti, K.S., Katti, D.R., 2006. Relationship of swelling and swelling pressure on silica-water  
544 interactions in montmorillonite. *Langmuir* 22(2), 532-537.

545 Kong, Y., Chen, X., Wang, W., Chen, Z., 2011. A novel palygorskite modified carbon paste  
546 amperometric sensor for catechol determination. *Anal. Chim. Acta* 688, 203-207.

547 Li, M.G., Ni, F., Wang, Y.L., Xu, S.D., Zhang, D.D., 2009. Sensitive and facile determination of  
548 catechol and hydroquinone simultaneously under coexistence of resorcinol with a Zn/Al layered  
549 double hydroxide film modified glassy carbon electrode. *Electroanalysis* 21, 1521-1526.

550 Lin, H., Gan, T., Wu, K., 2009. Sensitive and rapid determination of catechol in tea samples using  
551 mesoporous Al-doped silica modified electrode. *Food Chem.* 113,701-704.

552 Lu, L., Zhang, L., Zhang, X., Huan, S., Shen, G., Yu, R., 2010. A novel tyrosinase biosensor based on  
553 hydroxyapatite-chitosan nanocomposite for the detection of phenolic compounds. *Anal. Chim.*  
554 *Acta* 665,146-151.

555 Marrubini, G., Calleri, E., Coccini, T., Castoldi, A.F., Manzo, L., 2005. Direct analysis of phenol,  
556 catechol and hydroquinone in human urine by coupled-column HPLC with fluorimetric  
557 detection. *Chromatographia* 62, 25-31.

558 Mendelovici, E., 1973. Infrared study of attapulgite and HCl treated attapulgite, *Clays Clay Miner.*  
559 21, 115-119.

560 Mercier, L., Detellier C., 1995. Preparation, characterization and applications as heavy metals sorbents  
561 of covalently grafted thiol functionalities on the interlamellar surface of montmorillonite.  
562 *Environ. Sci. Technol.* 29(5), 1318-1323.

563 Moldoveanu, S.C., Kiser, M., 2007. Gas chromatography/mass spectrometry versus liquid  
564 chromatography/fluorescence detection in the analysis of phenols in mainstream cigarette  
565 smoke. *J. Chromatogr. A.* 1141(1), 90-97.

566 Montserrat, C.P., Xavier, M.B., Carole, C.B., Marty, J.M., 2010. Diazonium-functionalized  
567 tyrosinase-based biosensor for the detection of tea polyphenols. *Microchim. Acta* 171,187-193.

568 Nagaraja, P., Vasantha, R.A., Sunitha, K.R., 2001. A sensitive and selective spectrophotometric  
569 estimation of catechol derivatives in pharmaceutical preparations. *Talanta* 55(6), 1039-1046.

570 Nurchi, V.M., Pivetta, T., Lachowicz, J.I., Crisponi, G., 2009. Effect of substituents on complex  
571 stability aimed at designing new iron(III) and aluminum(III) chelators. *J. Inorg. Biochem.*  
572 103(2), 227-236.

573 Ozoner, S.K., Yalvac, M., Erhan, E., 2010. Flow injection determination of catechol based on  
574 polypyrrole-carbon nanotube-tyrosinase biocomposite detector. *Curr. Appl. Phys.* 10, 323-328.

575 Park, M., Shim, I.K., Jung, E.Y., Choy, J.H., 2004. Modification of external surface of laponite by  
576 silanegrafting. *J. Phys. Chem. Solids* 6(2), 499-501.

577 Piscitelli, F., Posocco, P., Toth, R., Fermeglia, M., Pricl, S., Mensitieri, G., Lavorgna, M., 2010.  
578 Sodium montmorillonite silylation: unexpected effect of the aminosilane chain length. *J. Colloid*  
579 *Interface Sci.* 351, 108-115.

580 Qin, Z., Yuan, P., Zhu J., He H., Liu D., Yang S., 2010. Influences of thermal pretreatment  
581 temperature and solvent on the organosilane modification of Al<sub>13</sub>-intercalated/Al-pillared  
582 montmorillonite. *Appl. Clay Sci.* 50 (4), 546-553.

583 Rodriguez, V.M.A., Gonzalez, L.J.D., Munoz, B.M.A., 1994. Acid activation of a Spanish sepiolite:  
584 physicochemical characterization, free silica content and surface area of products obtained. *Clay*  
585 *Miner.* 29, 361-367.

586 Shan, D., Zhang, J., Xue, H.-G., Zhang, Y.-C., Cosnier, S., Ding, S.-N., 2009. Polycrystalline bismuth  
587 oxide films for development of amperometric biosensor for phenolic compounds. *Biosens.*  
588 *Bioelectron.* 24, 3671-3676.

589 Shih, Y., Zen, J.M., Kumar, A.S., Chen, P.-Y., 2004. Flow injection analysis of zinc pyrithione in hair  
590 care products on a cobalt phthalocyanine modified screen-printed carbon electrode. *Talanta*  
591 62(5), 912-917.

592 Suarez B.M., Flores G.L.V., Vicente R.M.A., Martin J.M.P., 1995. Acid activation of a palygorskite  
593 with HCl: development of physico-chemical, textural and surface properties, *Appl. Clay Sci.*  
594 10, 247-258.

595 Su, L.N., Qi T., Hongping H., Jianxi Z., Peng Y., 2012. Locking effect: A novel insight in the  
596 silylation of montmorillonite surfaces. *Mater. Chem. Phys.* 136(2-3), 292-295.

597 Sun, W., Li Y.Z., Yang, M.X., Li, J., Jiao, K., 2008. Application of carbon ionic liquid electrode for  
598 the electrooxidative determination of catechol. *Sens. Actuator B-Chem.* 133, 387-392.

599 Temerk, Y.M., Ibrahim, H.S.M., Schuhmann, W., 2006.  
600 Cathodic adsorptive stripping voltammetric determination of the antitumor drug rutin in  
601 pharmaceuticals, human urine and blood serum. *Microchim. Acta* 153, 7-13.

602 Tonle, I.K., Ngameni, E., Walcarius, A., 2004. From clay to organoclay film modified electrodes:  
603 tuning charge selectivity in ion exchange voltammetry. *Electrochim. Acta* 49, 3435-3443.

604 Tonle, I.K., Ngameni, E., Tchieno, F.M.M., Walcarius A., 2015. Organoclay-modified electrodes:  
605 preparation, characterization and recent electroanalytical applications. *J. Solid State*  
606 *Electrochem.* 19, 1949-1973.

607 Tonle, K.I., Ngameni, E., Njopwouo, D., Carteret, C., Walcarius A., 2003. Functionalization of natural  
608 smectite-type clays by grafting with organosilanes: physico-chemical characterization and  
609 application to mercury (II) uptake. *Phys. Chem. Chem. Phys.* 5, 4951- 496.

610 Tonle, K.I., Ngameni, E., Walcarius, A., 2005. Preconcentration and voltammetric analysis of  
611 mercury(II) at a carbon paste electrode modified with natural smectite-type clays grafted with  
612 organic chelating groups. *Sens. Actuator B-Chem.* 110, 195-203.

613 Unnikrishnan, B., Ru, P.L., Chen, S.M., 2012. Electrochemically synthesized Pt-MnO<sub>2</sub> composite  
614 particles for simultaneous determination of catechol and hydroquinone. *Sens. Actuator B-Chem.*  
615 169, 235-242.

616 Van Olphen. H., Fritpiat. J.J., Data handbook for clay materials and other non-metallic  
617 minerals. Pergamon Press. 1979.

618 Wang, G., He, X., Zhou, F., Li, Z., Fang, B., Zhang, X., Wang, L., 2012. Application of gold  
619 nanoparticles/TiO<sub>2</sub> modified electrode for the electrooxidative determination of catechol in tea  
620 samples. *Food Chem.* 135, 446-451.

621 Wang, Z., Li, S.L.Q., 2007. Simultaneous determination of dihydroxybenzene isomers at single-wall  
622 carbon nanotube electrode. *Sens. Actuator B-Chem.* 127,420-425.

623 Xie, T., Liu, Q., Shi, Y., Liu, Q., 2006. Simultaneous determination of positional isomers of  
624 benzenediols by capillary zone electrophoresis with square wave amperometric detection. *J.*  
625 *Chromatogr. A* 1109, 317-321.

626 Xue, A., Zhou, S., Zhao, Y., Lu, X., Han P., 2011. Effective NH<sub>2</sub>-grafting on attapulgite surfaces for  
627 adsorption of reactive dyes. *J. Hazard. Mater.* 194, 7-14.

628 Yang, P., Zhu, Q.Y., Chen, Y.H., Wang, F.W., 2009. Simultaneous determination of hydroquinone  
629 and catechol using poly(p-aminobenzoic acid) modified glassy carbon electrode. *J. Appl.*  
630 *Polym. Sci.* 113, 2881-2886.

631 Yongqing, L., Jian, L., Yanjun, Z., 2017. Poly(sulfosalicylic acid)/multi-walled carbon nanotube  
632 modified electrode for the electrochemical detection of catechol. *Int. J. Electrochem. Sci.* 12,  
633 9512-9522.

634 Yuan, X., Yuan, D., Zeng, F., Zou, W., Tzorbatzoglou, F., Tsiakaras, P., Wang Y., 2013. Preparation  
635 of graphitic mesoporous carbon for the simultaneous detection of hydroquinone and catechol.  
636 *Appl. Catal. B Environ.* 129, 367-374.

637 Yue, X., Pang, S., Han, P., Zhang, C., Wang, J., Zhang, L., 2013. Carbon nanotubes/carbon paper  
638 composite electrode for sensitive detection of catechol in the presence of hydroquinone.  
639 *Electrochem. Comm.* 34, 356-359.

640 Zhao, D.-M., Zhang, X.-H., Feng, L.-J., Jia, L., Wang, S.-F., 2009. Simultaneous determination of  
641 hydroquinone and catechol at PASA/MWNTs composite film modified glassy carbon electrode.  
642 *Colloids Surf B: Biointerfaces* 74,317-321.

643 Zhao, Y., Song, X., Song, Q., Yin, Z., 2012. A facile route to the synthesis copper oxide/reduced  
644 graphene oxide nanocomposites and electrochemical detection of catechol organic pollutant.  
645 *Cryst. Eng. Comm.* 14, 6710-6719.

646

647  
648  
649  
650  
651  
652  
653  
654  
655  
656  
657  
658  
659  
660  
661  
662  
663  
664  
665  
666  
667  
668  
669  
670  
671  
672  
673

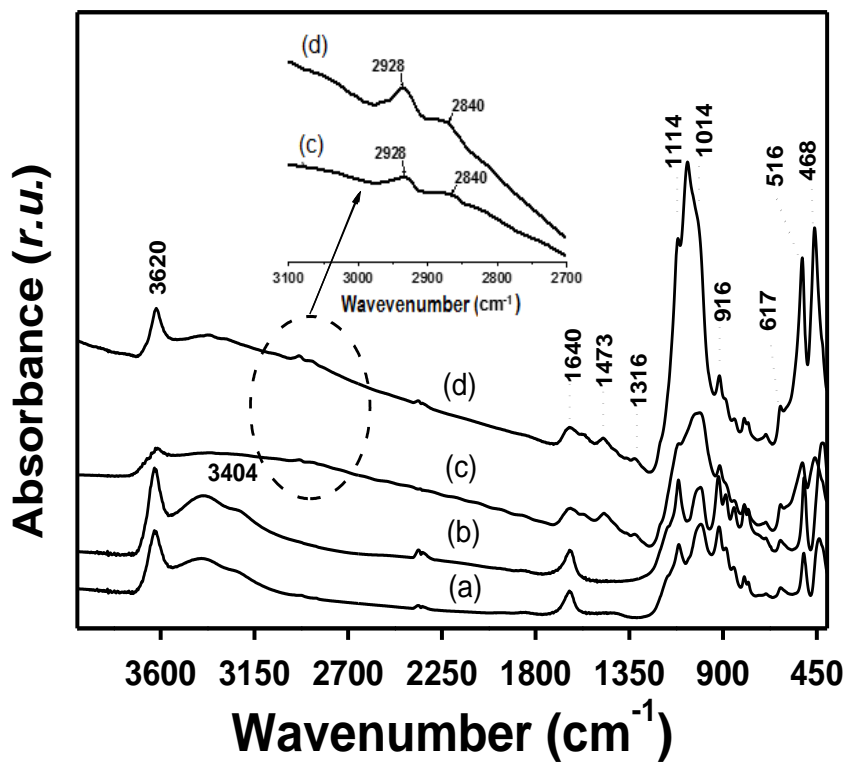


**Figure 1**

674  
675  
676  
677  
678  
679  
680  
681  
682  
683  
684  
685  
686  
687  
688  
689  
690  
691  
692  
693  
694  
695  
696  
697  
698  
699  
700

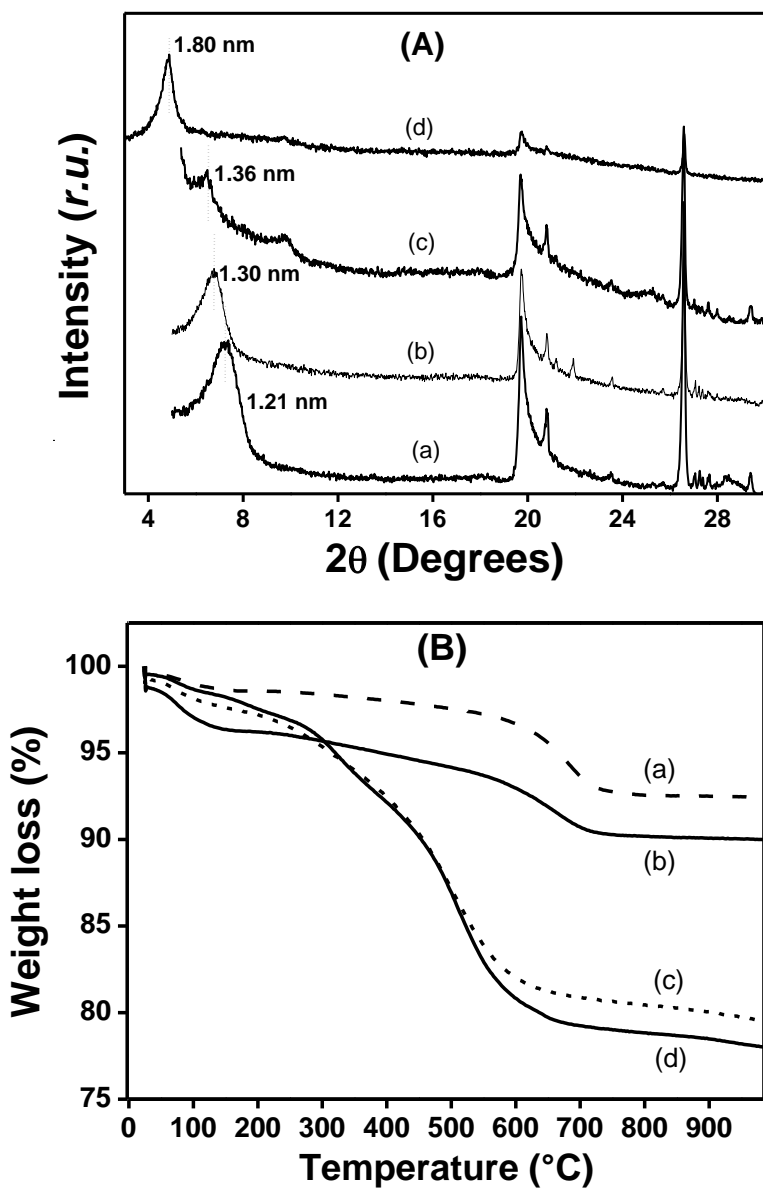
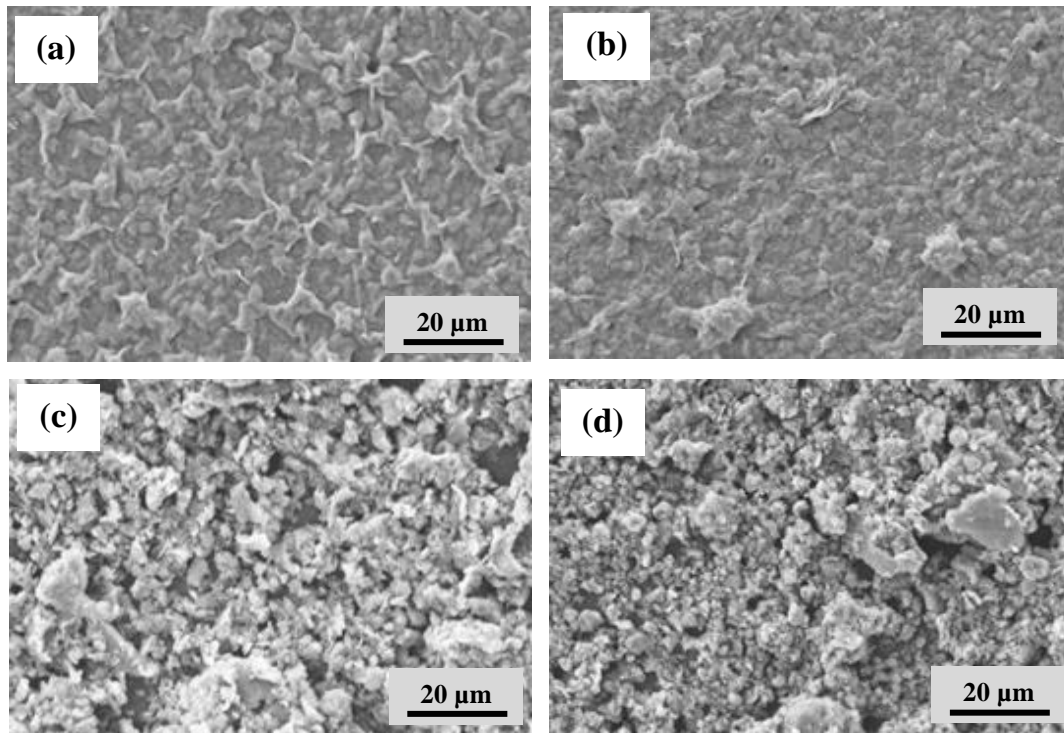


Figure 2

701  
702  
703  
704  
705  
706  
707  
708  
709  
710  
711  
712  
713  
714  
715  
716  
717  
718  
719  
720  
721  
722  
723  
724  
725  
726  
727  
728  
729  
730



**Figure 3**

731

732

733

734

735

736

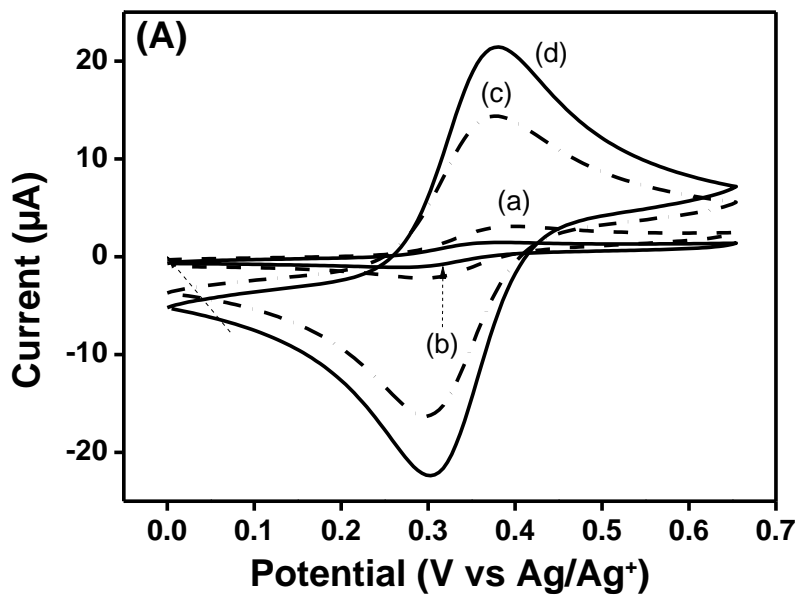
737

738

739

740

741



742

743

744

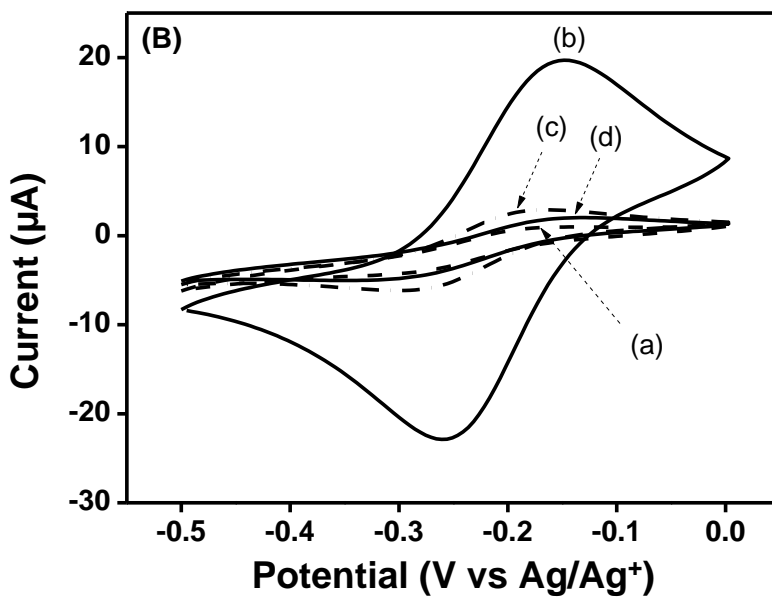
745

746

747

748

749



750

751

752

753

754

755

756

757

Figure 4

758  
759  
760  
761  
762  
763  
764  
765  
766  
767  
768  
769  
770  
771  
772  
773  
774  
775  
776  
777  
778  
779  
780  
781  
782  
783  
784

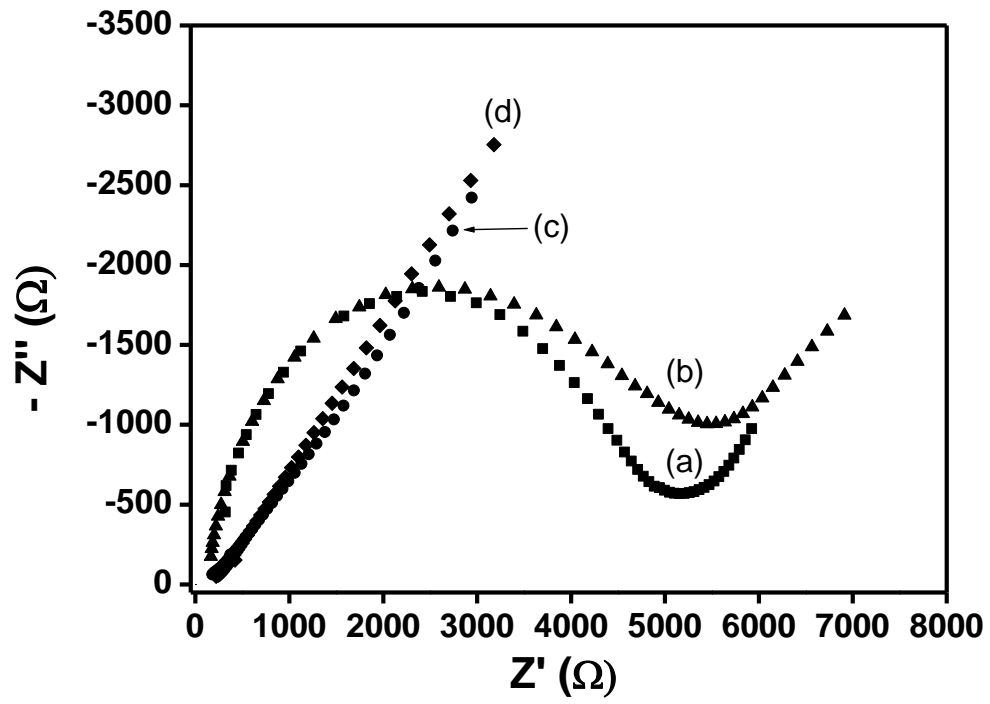
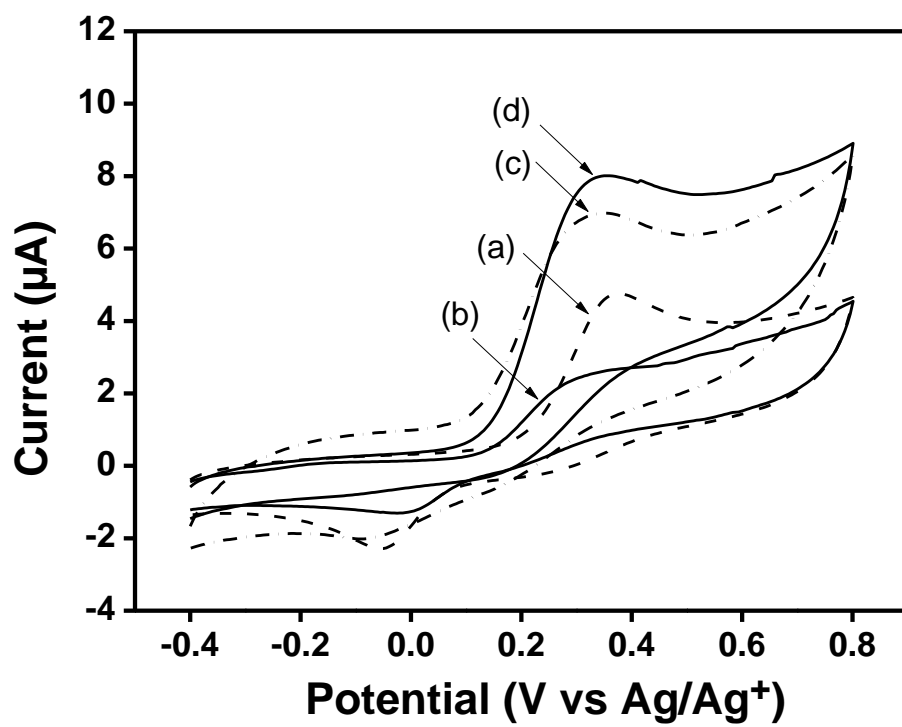


Figure 5

785

786



787

788

789

790

791

**Figure 6**

792

793

794

795

796

797

798

799  
800  
801  
802  
803  
804  
805  
806  
807  
808  
809  
810  
811  
812  
813  
814  
815  
816  
817  
818  
819  
820  
821  
822  
823  
824  
825

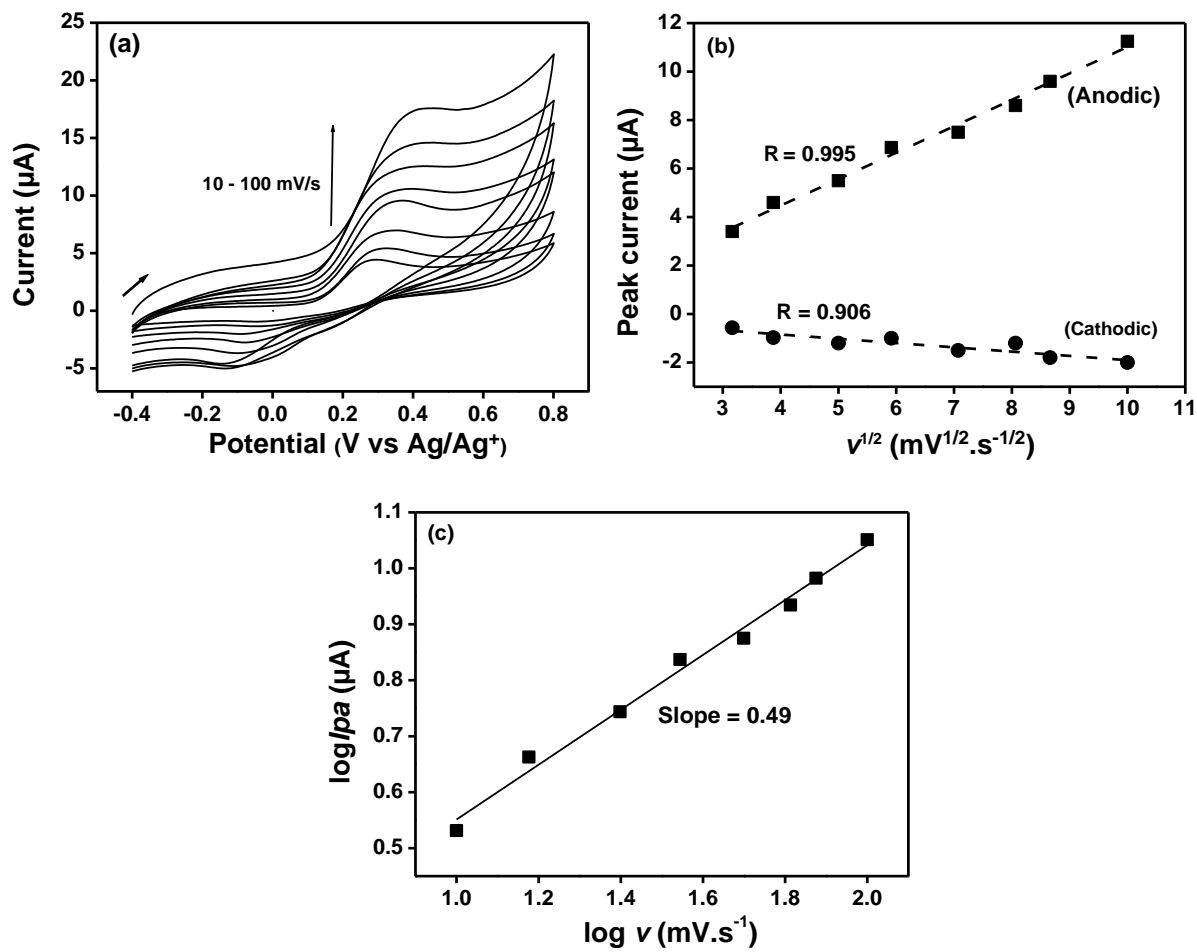
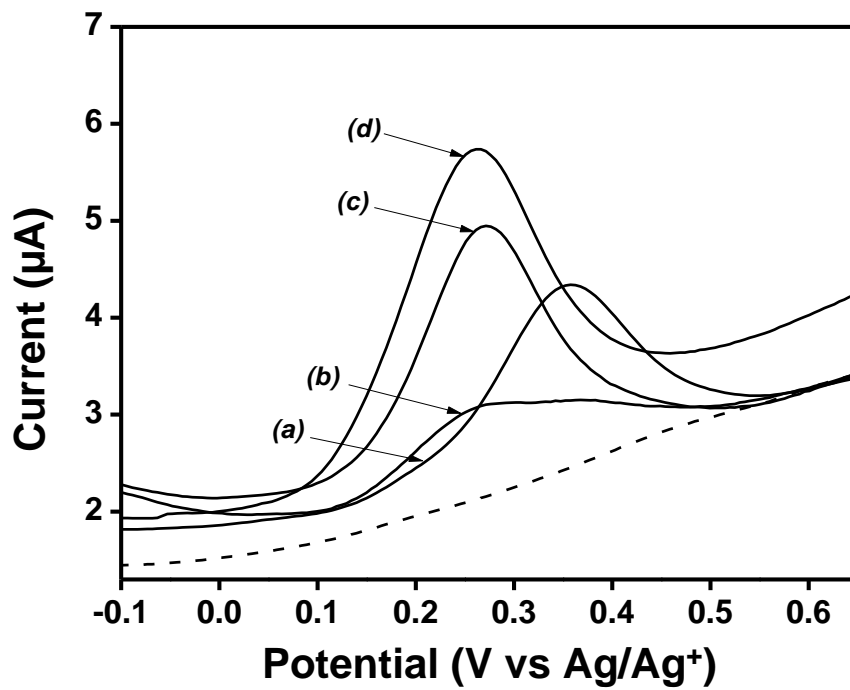


Figure 7

826  
827  
828  
829  
830  
831  
832  
833  
834  
835  
836  
837  
838  
839  
840  
841  
842  
843  
844  
845  
846  
847  
848  
849  
850  
851  
852



**Figure 8**

853  
854  
855  
856  
857  
858  
859  
860  
861  
862  
863  
864  
865  
866  
867  
868  
869  
870  
871  
872  
873  
874  
875  
876  
877  
878  
879  
880

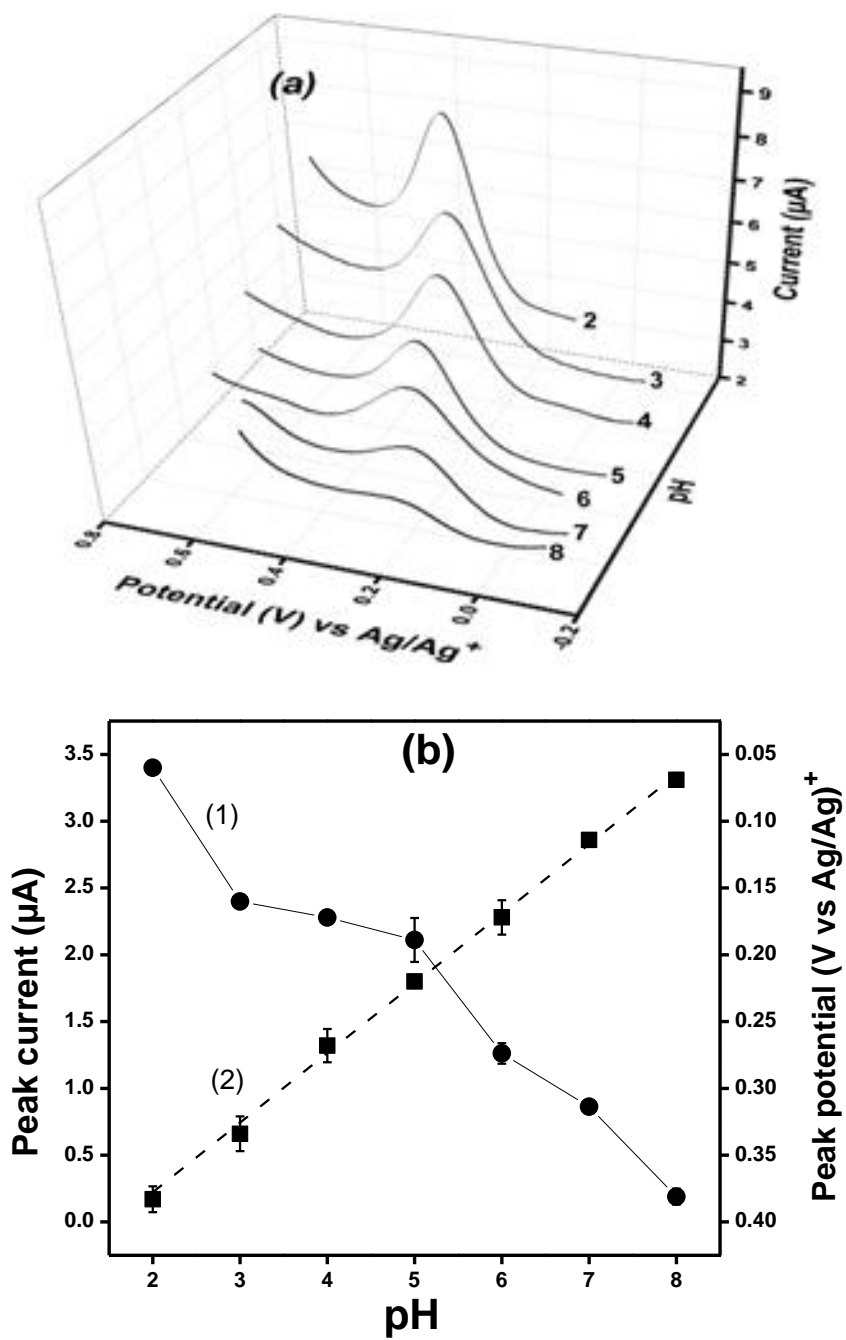
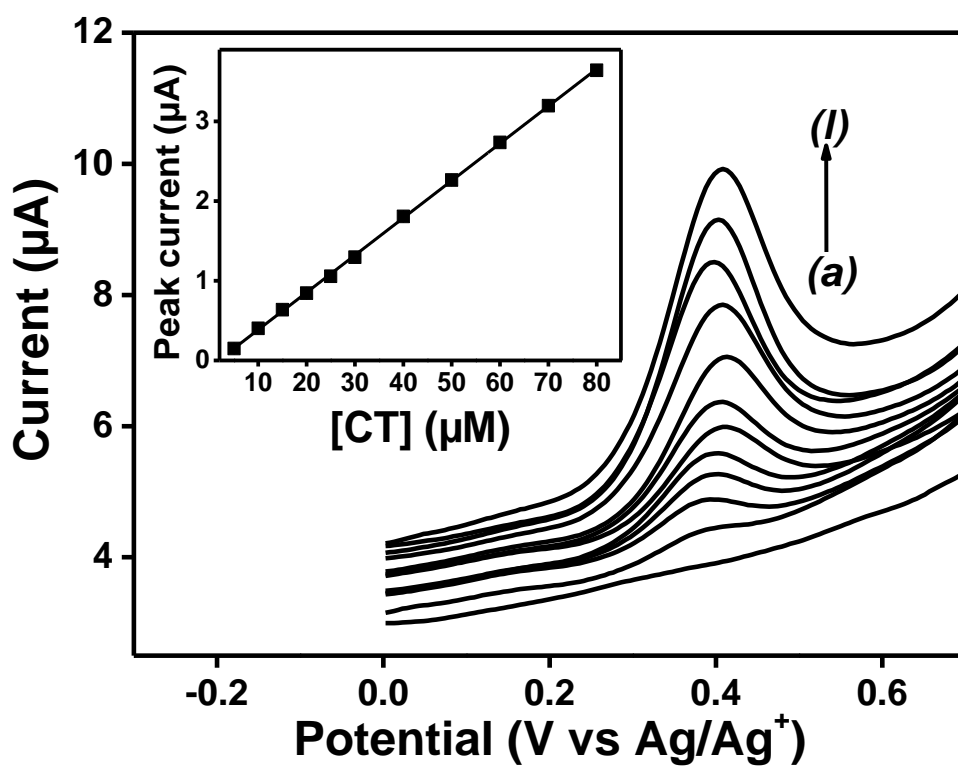


Figure 9

881  
882  
883  
884  
885



886  
887  
888  
889  
890  
891  
892  
893  
894  
895

Figure 10

896

## Figure caption

897

898 **Fig. 1.** Infrared spectra of raw (a): Mt-Na, (b): MtH, (c): Mt-NH<sub>2</sub> and (d): MtH-NH<sub>2</sub>.

899 **Fig. 2.** (A) Powdered X-ray diffraction patterns, and (B) TGA curves of (a): Mt-Na, (b): MtH,  
900 (c): Mt-NH<sub>2</sub> and (4): MtH-NH<sub>2</sub>.

901 **Fig. 3.** SEM micrographs of GCE covered with various films: (a): Mt-Na, (b): MtH, (c): Mt-  
902 NH<sub>2</sub> and (4): MtH-NH<sub>2</sub>.

903 **Fig. 4.** Cyclic voltammograms recorded in 0.1 M KCl/HCl (pH 1) containing (a) 0.5 mM  
904 [Fe(CN)<sub>6</sub>]<sup>3-</sup> and (b) 0.5 mM [Ru(NH<sub>3</sub>)<sub>6</sub>]<sup>3+</sup>, using various electrodes: (a) Bare GCE, (b)  
905 GCE/Mt-Na, (c) GCE/Mt-NH<sub>2</sub> and (d) GCE/MtH-NH<sub>2</sub>. The scan rate was 20 mV.s<sup>-1</sup>

906 **Fig. 5.** EIS spectra in 5 mM [Fe(CN)<sub>6</sub>]<sup>3-/4-</sup> with 0.1 M KCl at various electrodes; (a): bare  
907 GCE, (b): GCE/Mt-Na, (c): GCE/Mt-NH<sub>2</sub> and (d): GCE/MtH-NH<sub>2</sub>. Amplitude of the applied  
908 wave potential: 5 mV.

909 **Fig. 6.** Cyclic voltammograms recorded at 50 mV.s<sup>-1</sup> for 0.2 mM CT in 0.1 M BRB solution  
910 (pH 4) on (a): bare GCE, (b): GCE/Mt-Na, (c): GCE/Mt-NH<sub>2</sub> and (d): GCE/ MtH-NH<sub>2</sub>.

911 **Fig. 7.** (a) Cyclic voltammograms recorded for 0.2 mM CT in 0.1 M BRB solution (pH 4) on  
912 GCE/MtH-NH<sub>2</sub> at different scan rates (10, 15, 25, 35, 50, 65, 75 and 100 mV.s<sup>-1</sup>), (b) Peak  
913 current as a function of  $v^{1/2}$  and (c)  $\log(I_{pa})$  as a function of  $\log(v)$ .

914 **Fig. 8.** DPVs of 0.1 mM CT recorded in 0.1 M BRB solution (pH 4) on (a): bare GCE,  
915 (b): GCE/Mt-Na, (c): GCE/Mt-NH<sub>2</sub> and (d): GCE/MtH-NH<sub>2</sub> (c). Accumulation time: 5 s. The  
916 dot line represents the signal of the bare GCE in blank solution.

917 **Fig. 9.** (a) DPV curves of 0.1 mM CT (obtained in triplicate) in 0.1 M BRB solution on  
918 GCE/MtH-NH<sub>2</sub> at various pH; (b) effect of pH, (1): on the peak current and (2): on the peak  
919 potential. Accumulation time: 5 s.

920 **Fig. 10.** DPV curves recorded under optimized conditions in 0.1 M BRB solution (pH 2) on  
921 GCE/MtH-NH<sub>2</sub> for different concentrations of CT (a-l): 5, 10, 15, 20, 25, 30, 40, 50, 60, 70  
922 and 80  $\mu$ M. Accumulation time: 30 s. Inset shows the corresponding calibration graph.

923